AD-A128 822 THE PRESENTATION OF HIGH STRAIN-RATES ON DEFORMATION MECHANISM MAPS(U) CAMBRIDGE UNIV (ENGLAND) DEPT OF ENGINEERING P M SARGENT ET AL. MAR 83 1/1

UNCLASSIFIED CUED/C/MATS/TR.98 DAJA37-80-C-0333 F/G 11/6 NL

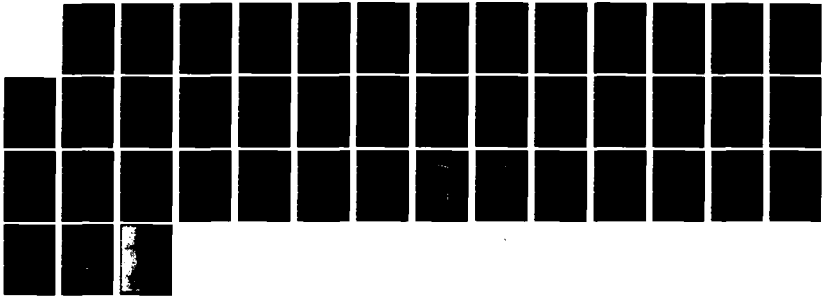

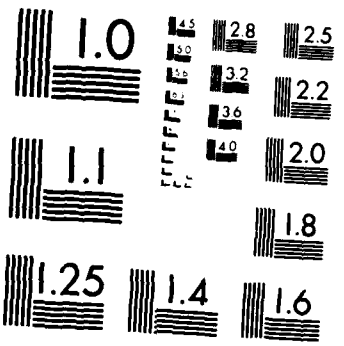

UNCLASSIFIED
SECURITY CLASSIFICATION OF THIS PAGE (When Data Entered)

R&D 2786-MS

REPORT DOCUMENTATION PAGE

READ INSTRUCTIONS BEFORE COMPLETING FORM

1. REPORT NUMBER	2. GOVT ACCESSION NO.	3. RECIPIENT'S CATALOG NUMBER
	AD-A128 822	

4. TITLE (and Subtitle)
The Presentation of High Strain-Rates on Deformation Mechanism Maps

5. TYPE OF REPORT & PERIOD COVERED
Final Technical Report
July 1980 - July 1982

6. PERFORMING ORG. REPORT NUMBER

7. AUTHOR(s)
P.M. Sargent and M.F. Ashby

8. CONTRACT OR GRANT NUMBER(s)
DAJA37-80-C-0333

9. PERFORMING ORGANIZATION NAME AND ADDRESS
Cambridge University, Engineering Department
Trumpington Street
Cambridge CB2 1PZ, U.K.

10. PROGRAM ELEMENT, PROJECT, TASK AREA & WORK UNIT NUMBERS
6.11.02A
1T16 1102BH57-04

11. CONTROLLING OFFICE NAME AND ADDRESS
USARDSG-UK
Box 65, FPO NY 09510

12. REPORT DATE
March 1983

13. NUMBER OF PAGES
39

14. MONITORING AGENCY NAME & ADDRESS(if different from Controlling Office)

15. SECURITY CLASS. (of this report)
Unclassified

15a. DECLASSIFICATION/DOWNGRADING SCHEDULE

16. DISTRIBUTION STATEMENT (of this Report)
Approved for public release; distribution unlimited

17. DISTRIBUTION STATEMENT (of the abstract entered in Block 20, if different from Report)

18. SUPPLEMENTARY NOTES

19. KEY WORDS (Continue on reverse side if necessary and identify by block number)

20. ABSTRACT (Continue on reverse side if necessary and identify by block number)

Phonon drag, power-law breakdown and the condition for adiabatic shear are expressed in terms of material properties, a critical strain-rate, and a critical strain. This information is incorporated into the construction of deformation-mechanism maps, which then show a field of drag-controlled plasticity and one of adiabatic shear (in which unstable flow may occur), together with the more usual fields of stable plasticity, power-law creep, diffusional flow and so forth. Where possible, the results have been compared with, and matched to, experiments.

DD FORM 1 JAN 73 1473 EDITION OF 1 NOV 65 IS OBSOLETE

UNCLASSIFIED
SECURITY CLASSIFICATION OF THIS PAGE (When Data Entered)

THE PRESENTATION OF HIGH STRAIN-RATES ON DEFORMATION MECHANISM MAPS

P.M. Sargent and M.F. Ashby

Cambridge University,
Engineering Department,
Trumpington Street,
CAMBRIDGE CB2 1PZ, U.K.

CUED/C/MATS/TR.98. March 1983

ABSTRACT

Phonon drag, power-law breakdown and the condition for adiabatic shear are expressed in terms of material properties, a critical strain-rate, and a critical strain. This information is incorporated into the construction of deformation-mechanism maps, which then show a field of drag-controlled plasticity and one of adiabatic shear (in which unstable flow may occur), together with the more usual fields of stable plasticity, power-law creep, diffusional flow and so forth. Where possible, the results have been compared with, and matched to, experiments.

TABLE 1: Symbols, Definitions and Units

σ	Tensile stress	(MN m^{-2})
σ_y	Tensile flow strength	(MN m^{-2})
σ_s	Shear stress	(MN m^{-2})
τ_o	Shear flow strength for obstacle cutting at O K	(MN m^{-2})
τ_p	Shear lattice resistance of Peierls stress at O K	(MN m^{-2})
ΔF_o	Obstacle cutting activation energy	(J)
ΔF_p	Lattice resistance activation energy	(J)
ε	Tensile strain	
ε_c	Critical tensile strain for shear localisation	
ε_o	Standard strain in the strain hardening constitutive equation	
$\dot{\varepsilon}$	Tensile strain-rate	(s^{-1})
$\dot{\varepsilon}_A$	Tensile strain-rate above which conditions are sensibly adiabatic	(s^{-1})
$\dot{\varepsilon}_o$	Obstacle controlled glide parameter, $= \dot{\gamma}_o/\sqrt{3}$	(s^{-1})
$\dot{\varepsilon}_s$	Standard strain-rate used to measure m	(s^{-1})
$\dot{\gamma}$	Shear strain-rate	(s^{-1})
$\dot{\gamma}^*$	Relativistic shear strain-rate limit	(s^{-1})
$\dot{\gamma}_o$	Obstacle controlled glide parameter, usually 10^6	(s^{-1})
$\dot{\gamma}_p$	Lattice resistance control parameter, usually 10^{11}	(s^{-1})
$\dot{\gamma}_D$	Drag limited shear strain-rate	(s^{-1})
$\dot{\gamma}_{R-D}$	Drag and relativistically limited shear strain-rate	(s^{-1})
$\dot{\gamma}_1$	Power-law creep shear strain-rate	(s^{-1})
$\dot{\gamma}_2$	Breakdown-modified power-law creep shear strain-rate	(s^{-1})
$\dot{\gamma}_3$	Low-temperature power-law creep shear strain-rate	(s^{-1})
$\dot{\gamma}_4$	Low-temperature, breakdown-modified power-law shear strain-rate	(s^{-1})
β	Normalised stress at which power-law breakdown occurs	
A,n	Power-law creep materials parameters	
m	Strain hardening exponent	
σ_o	Strain hardening pre-exponent	(MN m^{-2})
B	Total drag coefficient	(MN m^{-2} s)
B_o	Electron drag coefficient	(MN m^{-2} s)
B	Phonon drag coefficient	(MN m^{-2} s)

T	Temperature (absolute)	(K)
T_s	Heat sink temperature (absolute)	(K)
ΔT	Temperature rise due to homogeneous heating	(K)
C_p	Volume specific heat	(J m^{-3} K^{-1})
K	Thermal conductivity	(J m^{-1} s^{-1} K^{-1})
k	Boltzmann's constant 1.38×10^{-23}	(J K^{-1})
τ	Characteristic time for thermal diffusion	(s)
R	Characteristic dimension of experimental specimen	(m)
A	Surface area of specimen	(m^2)
V	Volume of specimen	(m^3)
α	Geometrical constant describing the shape of the specimen	
$\dot{Q}$	Rate of heat input per unit volume	(J m^{-3} s^{-1})
$\dot{q}$	Rate of heat loss through the surface	(J m^{-2} s^{-1})
D_v	Volume diffusivity	(m^2 s^{-1})
D_{core}	Dislocation core diffusivity	(m^2 s^{-1})
D_b	Grain boundary diffusivity	(m^2 s^{-1})
D_{eff}	Effective diffusivity in power-law creep	(m^2 s^{-1})
D'_{eff}	Effective diffusivity in diffusion creep	(m^2 s^{-1})
d	Grain size	(m)
δ	Grain boundary 'thickness'	(m)
a_c	Dislocation core 'cross-section'	(m^2)
π	Geometrical dimensionless constant, about 3	
Ω	Atomic volume	(m^3)
ϕ	Normalised thermal softening parameter (eqn. 17)	
v	Dislocation velocity	(m s^{-1})
b	Magnitude of Burgers vector	(m)
μ	Shear modulus	(MN m^{-2})
ρ	Mobile dislocation density	(m^{-2})

1. INTRODUCTION: DEFORMATION MECHANISMS

A deformation mechanism map is a way of summarising data for, and the understanding of, the plastic properties of a material. It is constructed by fitting model-based rate equations for each mechanism of plasticity to data for the material: yield data, data for diffusion, and so forth. A large number of maps are now available (see, for example, Frost and Ashby, 1982). But all are limited, both by the data and by the models used to construct them, to strain-rates of less than 1/s. Metal working and machining operations (such as wire drawing, turning, drilling), punching, guillotining, and the impact of projectiles, generate strain-rates which are much higher than this. Then new mechanisms appear, and others are modified.

At low temperatures (0 to 0.35 T_M, where T_M is the melting temperature), strength at low strain-rates is determined by obstacles to dislocation glide: by the lattice resistance, by a solid solution, by a precipitate or dispersion, or by work-hardening. But at high strain-rates this can change: the interaction of the rapidly-moving dislocations with phonons, or (at very low temperatures) with electrons, generates a *phonon (or electron) drag* which determines the flow strength. And at very high strain-rates (of order 10^6/s) the compression of the elastic field ahead of the dislocation, now moving at near-sonic velocities, causes its effective mass to increase, and the flow strength to rise steeply. This *relativistic limit* is rarely approached, but drag-limited flow is encountered at strain-rates which are achieved in machining, punching and impact loading.

At higher temperatures ($\gtrsim$ 0.35 T_M), materials at modest strain-rates exhibit power-law creep. But above rates which may be as low

as 10^{-4}/s, the power-law breaks down. This *power-law breakdown* is really a broad transition from the "creeping" response to the "yielding" response to stress, characteristic of low temperatures. Hot-working operations almost all involve strain-rates that lie in this regime, so it is important to incorporate it into any treatment of high strain-rates.

When solids are deformed fast enough that the work of deformation, which appears as heat, does not have time to diffuse out, then they may show a localisation of slip known as *adiabatic shear*. Analyses of this problem vary in generality and complexity, but almost all are based on the same physical idea: that if the loss of strength due to heating exceeds the gain in strength due to the combined effects of strain and of strain-rate (which are locally higher if deformation becomes localised), then localisation of adiabatic shear will occur.

We survey here the understanding by these strain-rate mechanisms, and develop ways of incorporating them into deformation mechanism maps.

2. MECHANISMS FOR UNIFORM FLOW

2.1 *Phonon Drag and Electron Drag, and the Relativistic Limit*

Above O K, moving dislocations interact with, and scatter, phonons which thereby exert a drag on it. As the temperature increases, the phonon density rises and the drag increases. Experimental data (see, for example, the review of Kocks et al., 1975) shows much scatter, but is generally consistent with a drag which increases linearly with temperature. Then the dislocation moves with velocity:

$$v = \frac{\sigma_s b}{B} \qquad (1)$$

$$B = B_1 \frac{T}{300} + B_o$$

where B is the total drag coefficient, B_1 the contribution of phonon drag at room temperature and B_o the (residual) electron drag coefficient at 0 K. Here σ_s is the shear stress, b the Burger's vector and T the absolute temperature.

The shear strain-rate $\dot{\gamma}$ is related to v by the Orowan equation*:

$$\dot{\gamma} = \rho\, b\, v$$

If, as the experiments suggest, the dislocation density ρ becomes independent of stress at high stresses, we find the drag-limited strain-rate:

$$\dot{\gamma}_D = \left(\frac{\rho\, b^2\, \mu}{B_1\, T/300 + B_o}\right) \frac{\sigma_s}{\mu} = C\, \frac{\sigma_s}{\mu} \qquad (2)$$

We have estimated the value of C at room temperature to be $(5.2 \pm 1) \times 10^6\ s^{-1}$ from the experimental results for copper and aluminium of Kumar et al., (1968) and Kumar and Kumble (1969), Here μ is the shear modulus, a convenient normalising parameter.

When dislocation velocities approach that of sound, the stress required increases more rapidly than the simple linear law predicts. This is in part due to the relativistic contraction of the strain field of the dislocation which causes its elastic energy to increase rapidly. If the dislocation density, too, approaches a limiting value at very high strain-rates, there exists a strain-rate limit also. Strain-rates greater than $10^6\ s^{-1}$ are not reported so we

---

*Most of the equations and figures of this paper are expressed in terms of shear stress, σ_s, and shear strain-rate, $\dot{\gamma}$. When equations are quoted, they are sometimes given as the more familiar relation between tensile stress σ and strain-rate $\dot{\epsilon}$. The two schemes are related by $\sigma_s = \sigma/\sqrt{3}$ and $\dot{\gamma} = \sqrt{3}\, \dot{\epsilon}$.

have taken this as the limit ($\dot{\gamma}^*$) and used the relativistic equation to predict the strain-rate limited by both drag and relativistic effects ($\dot{\gamma}_{R-D}$):

$$\dot{\gamma}_{R-D} = \frac{\dot{\gamma}_D}{(1 + (\dot{\gamma}_D/\dot{\gamma}^*)^2)^{\frac{1}{2}}} \tag{3}$$

These mechanisms are poorly investigated, and the data for them are meagre and uncertain. They are included in order to show, approximately, the regimes on the deformation maps where drag should be important.

2.2 *Power-Law Breakdown*

Above about $\frac{1}{3}\ T_M$ (where T_M is the melting point) metals start to creep. The power-law which describes steady-state creep in this regime breaks down when stresses exceed about $10^{-3}\ \mu$. Then the noramlly accepted power-law creep equation:

$$\dot{\gamma}_1 = A\ D_v \frac{\mu b}{kT} \left(\frac{\sigma_s}{\mu}\right)^n \tag{4}$$

where A and n are dimensionless creep constants, tabulated for a wide range of materials by Frost and Ashby (1982), must be modified. A satisfactory modification giving an adequate fit to experimental data in both the power-law and the breakdown regime above about $0.5\ T_M$ is:

$$\dot{\gamma}_2 = A\ D_v \frac{\mu b}{kT} [\beta \sinh (\sigma_s/\mu\beta)]^n \tag{5}$$

Here β is the normalised stress at which deviation from the power-law is observed. For pure copper and aluminium β is found to be about 10^{-3}, for the b.c.c. transition metal tungsten, a value of 5×10^{-4} fits the data better (Frost and Ashby, 1982) and for h.c.p. α-titanium a value of 6×10^{-3} has been found (Doner and Conrad, 1973).

At lower temperatures in the power-law regime, diffusion along dislocation cores makes a greater contribution to the creep rate than lattice diffusion. Then eqn. (4) is modified (Frost and Ashby, 1982) to:

$$\dot{\gamma}_3 = 10A \left(\frac{a_c}{b^2}\right) D_{core} \frac{\mu b}{kT} \left(\frac{\sigma_s}{\mu}\right)^{n+2} \tag{6}$$

and eqn. (5) to:

$$\dot{\gamma}_4 = 10A \left(\frac{a_c}{b^2}\right) D_{core} \frac{\mu b}{kT} \left(\beta \sinh \left(\sigma_s/\mu\beta\right)\right)^n \left(\frac{\sigma_s}{\mu}\right)^2 \tag{7}$$

3. NON-HOMOGENEOUS FLOW: ADIABATIC SHEAR

Deformation generates heat, causing the flow strength σ_y to fall. Work-hardening, or an increase in strain-rate, raises σ_y. The classical treatment of diffuse necking (Considere, 1885) postulates that instability starts when the rate of softening first exceeds the rate of hardening. If the current flow strength σ_y depends on strain, ε, strain-rate, $\dot{\varepsilon}$, and temperature, T:

$$\sigma_y = \sigma_y \left(\varepsilon, \dot{\varepsilon}, T\right) \tag{8}$$

then the total differential of σ_y is zero at the instability point:

$$d\sigma_y = \left(\frac{\partial \sigma_y}{\partial \varepsilon}\right)_{T,\dot{\varepsilon}} d\varepsilon + \left(\frac{\partial \sigma_y}{\partial T}\right)_{\varepsilon,\dot{\varepsilon}} dT + \left(\frac{\partial \sigma_y}{\partial \dot{\varepsilon}}\right)_{\varepsilon,T} d\dot{\varepsilon} = 0 \qquad (9)$$

This is the starting point of most treatments of adiabatic instability (see, for instance, Zener and Holloman, 1944; Backofen, 1964; Baron, 1956; Culver, 1973; Argon, 1973; or Staker, 1981).

There are two useful limiting cases. At temperatures below those of creep, $\frac{d\sigma_y}{d\varepsilon} >> \frac{d\sigma_y}{d\dot{\varepsilon}}$. Then:

$$\left(\frac{\partial \sigma_y}{\partial \varepsilon}\right)_{T,\dot{\varepsilon}} = - \left(\frac{\partial \sigma_y}{\partial T}\right)_{\varepsilon,\dot{\varepsilon}} \frac{dT}{d\varepsilon} \qquad (10)$$

In words: the decrease in flow strength caused by heating (due to the plastic work) balances its increase with strain (Fig. 1). The other limit is that of *steady state*. Then $\frac{d\sigma_y}{d\varepsilon} = 0$, giving:

$$\left(\frac{\partial \sigma_y}{\partial \dot{\varepsilon}}\right)_{T,\varepsilon} = - \left(\frac{\partial \sigma_y}{\partial T}\right)_{\dot{\varepsilon},\varepsilon} \frac{dT}{d\dot{\varepsilon}} \qquad (11)$$

In words: the decrease in flow stress caused by heating (due to the plastic work) is just balanced by its increase with strain-rate.

3.1 *Purely Adiabatic Conditions (No Heat Loss)*

At sufficiently high strain-rates ($\dot{\varepsilon} > \dot{\varepsilon}_A$, defined below), all mechanical work is converted into heat, so that heat is generated at the rate:

$$\dot{Q} = \sigma_y \dot{\varepsilon} \tag{12}$$

per unit volume per second. If heating is uniform, we have:

$$\left.\begin{aligned} dQ &= \sigma_y \, d\varepsilon \\ &= C_p \, dT \end{aligned}\right\} \tag{13}$$

giving:

$$\frac{dT}{d\varepsilon} = \frac{\sigma_y}{C_p} \tag{14}$$

At low temperatures we can assume (as Staker, 1981, does) that $(\partial\sigma_y/\partial\dot{\varepsilon})$ is negligible. If, further, we describe the stress-train curve by:

$$\sigma_y = \sigma_o \left(\frac{\varepsilon}{\varepsilon_o}\right)^m \tag{15}$$

we obtain the strain for the onset of instability under *purely adiabatic conditions* (when $\dot{\varepsilon} > \dot{\varepsilon}_A$, defined below) as:

$$\varepsilon_c = \frac{-\, m\, C_p}{\left(\frac{\partial\sigma_y}{\partial T}\right)_{\varepsilon,\dot{\varepsilon}}} \tag{16}$$

This is essentially identical to the results of Culver (1973), Bai (1981) and Staker (1981). It is helpful to rewrite it as:

$$\varepsilon_c = \frac{m\, C_p\, T_M}{\phi\, \sigma_y} \tag{17}$$

where

$$\phi = -\frac{T_M}{\sigma_y}\left(\frac{\partial \sigma_y}{\partial T}\right)_{\varepsilon,\dot{\varepsilon}}$$

The quantity ϕ is a dimensionless material property. Typical values for it are given in Table 2: it lies in the range:

$$\phi = 0.5 \text{ to } 6 \tag{18}$$

The smaller number is appropriate if the yield stress has the same temperature dependence as the modulus. The larger number is typical of a very temperature-dependent material. For most engineering metals, the value is approximately between 1 and 3, depending on temperature and strain-rate. Then the critical strain ε_c depends mainly on the current strength σ_y, the work-hardening exponent, m, the specific heat C_p and the melting point T_M.

Eqn. (17) shows that ε_c has a slight dependence on strain-rate, through the strain-rate dependence of m and of σ_y. This is important since it affects how the boundary of the adiabatic shear field is displayed: if ε_c varies with strain-rate, then both ε_c and $\dot{\varepsilon}_A$ must be evaluated using the value of σ_y and m corresponding to the strain ε_c and the strain-rate $\dot{\varepsilon}_A$.

3.2 *Effect of Heat Loss on the Adiabatic Conditions*

Eqn. (17) defines a sufficient condition for the onset of adiabatic shear provided no heat is lost from the sample. It is the basis of the approach used by Culver (1973) and of Staker (1981) who supports it with data on explosively deformed ($\dot{\varepsilon} \simeq 10^4$/s) AISI 4340 steel, heat treated to give various combinations of σ_y and m. The assumption of no heat loss is valid, of course, only when the rate of deformation is sufficiently large. We now estimate this critical strain-rate $\dot{\varepsilon}_A$ and examine the criterion for adiabatic shear, allowing for heat loss.

Consider a uniform deformation (and thus heat input) but with heat loss to the surroundings at a rate $\dot{q}$ (J m^{-2} s^{-1}) (Carslaw and Jaeger, 1959, or Geiger and Poirier, 1973, Ch. 7):

$$\dot{q} = \frac{\alpha K}{R} (T - T_s) \tag{19}$$

Here α is a constant of order 2, K is the thermal conductivity (J m^{-1} s^{-1} K^{-1}) and R (m) a characteristic dimension of the sample (e.g. the radius of a cylindrical sample if conduction to the environment is important, or the spacing of slip bands if deformation is not homogeneous, see Fig. 2. T is the temperature of the sample and T_s is that of the heat sink (which will be the bulk specimen temperature in the 'slipband' case.)

The heat balance equation now becomes:

$$V C_p \, dT + A \, \dot{q} \, dt = V \, \sigma_y \, d\varepsilon \tag{20}$$

where V is the volume of the sample and A its surface area (Estrin and Kubin, 1980, base their analysis on this equation). Taking A/V = 2/R we find:

$$\frac{dT}{dt} + \frac{2\,\alpha\,K}{C_p\,R^2}\,(T - T_s) = \sigma_y \qquad \frac{\dot{\varepsilon}}{C_p} \tag{21}$$

Now, the factor $\frac{C_p\,R^2}{2\alpha K} = \tau$ is the characteristic time (in seconds) for thermal diffusion. Equation (21) now becomes:

$$\frac{dT}{d\varepsilon} + \frac{1}{\tau\dot{\varepsilon}}\,(T - T_s) = \frac{\sigma_y}{C_p} \tag{22}$$

It cannot be integrated analytically because σ_y depends on strain according to the power-law, eqn. (15).

Consider first the approximate solution to this equation. If the critical strain required for adiabatic shear is ε_c, we may write:

$$\frac{dT}{d\varepsilon} \simeq \frac{T - T_s}{\varepsilon_c}$$

Heat loss to the surroundings becomes important only if the second term on the left hand side of eqn. (22) becomes comparable to, or larger than, the first. We therefore have adiabatic conditions only when:

$$\frac{T - T_s}{\varepsilon_c} \geq \frac{T - T_s}{\tau \dot{\varepsilon}}$$

giving (from the definitions of τ and ε_c) critical strain-rates which must be exceeded for adiabatic shear to become possible:

$$\dot{\varepsilon}_A = \frac{\varepsilon_c}{\tau} = \frac{2m \alpha K T_M}{\phi \sigma_y R^2} \qquad (23)$$

where σ_y, ϕ and m are the values at the strain ε_c and the strain-rate $\dot{\varepsilon}_A$.

In the *steady state* limit, appropriate to higher temperatures, $dT/d\varepsilon$ is zero, giving (from eqn. 22):

$$T = T_s + \frac{\sigma_y}{C_p} \tau \dot{\varepsilon} \qquad (24)$$

or

$$\frac{dT}{d\dot{\varepsilon}} = \frac{\sigma_y \tau}{C_p} \qquad (25)$$

Combining this with the localisation condition (eqn. 11) and the constitutive law for power-law creep (eqn. 4):

gives

$$\dot{\varepsilon}_A = \frac{2 \alpha K T_M}{n \phi \sigma_y R^2} \qquad (26)$$

which is identical with eqn. (23) with m replaced by $\frac{1}{n}$. If σ_y is set equal to the "saturation" or limiting strength at large strain at low temperatures, or the steady creep stress at high, then. eqn. (26)

defines (approximately) a minimum strain-rate below which adiabatic shear will not occur.

We thus find that for shear localisation under true *adiabatic conditions* (no heat loss), two conditions must be met simultaneously: the strain must exceed the critical strain, given by eqn. (18), and the strain-rate must exceed the critical rate given by eqn. (23) or (26).

3.3 *Homogeneous Heating*

Because both conditions must be satisfied, a homogeneous deformation ε_c preceeds localisation, even when the strain-rate exceeds $\dot{\varepsilon}_A$. During this homogeneous strain, the temperature of the sample rises by ΔT where (Fig. 3):

$$\Delta T \simeq 0.5 \frac{\sigma_y}{C_p} \varepsilon_c \qquad (27)$$

using eqn. (17):

$$\frac{\Delta T}{T_M} = \frac{0.5\ m}{\phi}$$

The strain hardening parameter m decreases monotonically with temperature for pure metals and alloys from a value near 0.5 at 0 K approaching a value near zero at higher temperatures (about $0.3\ T_M$) where recovery mechanisms are rapid. Using data from Table 2, $\Delta T/T_M$ varies from a maximum of 0.5 to as little as 0.005. Clearly, the larger value means that the homogeneous heating before instability is large, and requires a correction to the equations. But the materials *most susceptible* to adiabatic shear (see Table 2) have low values of m and

large values of ϕ, so that the precursory temperature-rise is small.

4. DEFORMATION-MECHANISM MAPS EXTENDED TO HIGH STRAIN-RATES

4.1 Construction of the Maps

Deformation-mechanism maps are constructed from constitutive equations, each describing one mechanism of deformation. The equations are based, as far as possible, on physical models for each mechanism, so justifying their extrapolation beyond the range of the data to which they are fitted. The models and procedure, are described in detail by Frost and Ashby (1982). Briefly, the maps are based on equations and data for *lattice-resistance controlled glide*:

$$\dot{\gamma} = \dot{\gamma}_p \left(\frac{\sigma_s}{\mu}\right)^2 \exp\left\{-\frac{\Delta F_p}{kT}\left(1 - \left(\frac{\sigma_s}{\hat{\tau}_p}\right)^{\frac{3}{4}}\right)^{\frac{4}{3}}\right\} \tag{28}$$

for *obstacle-controlled glide:*

$$\dot{\gamma} = \dot{\gamma}_o \exp\left\{-\frac{\Delta F_o}{kT}\left(1 - \frac{\sigma_s}{\hat{\tau}_o}\right)\right\} \tag{29}$$

for *power-law creep:*

$$\dot{\gamma} = \frac{A\, D_{eff}\, \mu b}{kT}\left(\frac{\sigma_s}{\mu}\right)^n \tag{30}$$

where

$$D_{eff} = D_v + 10\,\frac{a_c}{b^2}\left(\frac{\sigma_s}{\mu}\right)^2 D_{core}$$

and for *diffusional flow:*

$$\dot{\gamma} = \frac{42\ \sigma_s\ \Omega}{kT\ d^2}\ D'_{eff} \qquad (31)$$

where $$D'_{eff} = D_v + \frac{\pi\delta}{d} D_b$$

The symbols are defined in Table 1. The procedure identifies the *dominant mechanism* (the one which, at a given stress and temperature, determines the strain-rate) and the *total strain-rate*, allowing for simultaneous contributions from independent mechanisms. The results are plotted as a map on axes of normalised stress (σ_s/μ) and temperature (T/T_M) or strain-rate $(\dot{\gamma})$ and stress (σ_s/μ).

For the present purposes, a new kind of map with axes of strain-rate $(\dot{\gamma})$ and temperature (T/T_M) is more helpful because it expands the high strain-rate regime while still allowing the others to be displayed. Phonon drag and the relativistic limit are incorporated as new mechanisms, using eqns. (2) and (3): the *slowest* of eqns. (2), (3), (28) and (29) is dominant, provided it is *faster* than the independent mechanisms described by eqns. (30) and (31). Power-law breakdown is included by replacing eqn. (30) by those of Section 2.2, which are conveniently combined into the single equation:

$$\dot{\gamma} = A\ D_{eff}\ \frac{\mu b}{kT}\ \left(\beta \sinh\ \left(\frac{\sigma_s}{\mu\beta}\right)\right)^n \qquad (32)$$

Only adiabatic shear produces special problems. Two conditions - a critical strain and a critical strain-rate - must be met simultaneously. It is straightforward to plot the critical strain-rate (eqn. 23):

$$\dot{\gamma} = \frac{2 m \alpha K T_M}{\phi \sigma_s R^2} \qquad (33)$$

It bounds the field in which adiabatic shear is possible. But displaying within that field the strain which must be exceeded for shear to occur is more difficult. We return to this problem in a moment.

Figs. 4 and 5 show maps for titanium and zirconium, using this procedure. Data are from Sargent and Ashby (1982). (The critical strain-rate was evaluated by the method described in Appendix 1 using a critical shear band spacing of 250 μm and the data in Table 3. The figures show the normal fields of glide plasticity, power-law creep and diffusional flow. But in addition there are fields of drag-controlled plasticity, power-law breakdown and adiabatic shear. The diagrams are bounded at the top by the relativistic limit. The data used to evaluate the adiabatic shear field are given in Appendix 2.

4.2 *Refinements: The Critical Strain*

Figs. 6 and 7 show the adiabatic shear fields in more detail. They were computed using the numerical method of Appendix 1. Boundaries for the onset of adiabatic shear are marked for unlimited strain (full heavy line) and at strains of 0.4 and 0.3 (thinner lines). Larger strains are needed to induce unstable shear at low strain-rates to compensate for the greater loss of heat. Larger strains are also required above 0.3 T_M in titanium because ϕ becomes small (see Appendix 1(b)).

The numerical computation of the conditions for instability is easier than solving the equations directly, but it obscures the physical understanding of the way in which the material parameters influence the results. Figure 8 shows an adiabatic shear field in α-titanium, bounded by the critical strain rate: $\dot{\varepsilon}_A = \varepsilon_c/\tau$ (R = 250 μm) using data for ϕ, σ_y

and m calculated for that same strain-rate. (Data are discussed in Appendix 2.) An approximate description of the adiabatic shear field is possible without simulation. From eqn. (23) or (26), the important parameters are the thermal softening rate, the strain hardening index and the thermal conductivity. To a reasonable approximation, the field boundary can be described by:

$$\dot{\varepsilon}_A\ (T) = \dot{\varepsilon}^o_A \frac{m}{m_o} \frac{K}{K_o} \frac{(-\partial\sigma/\partial T)_o}{(-\partial\sigma/\partial T)} \qquad (34)$$

where m, K and $(\partial\sigma_y/\partial T)$ are the values at temperature T and m_o, $\dot{\varepsilon}^o_A$ K_o and $(\partial\sigma_y/\partial T)_o$ are the values at 300 K. It has been used to construct Fig. 9. We now examine the temperature dependence of the quantities which enter it.

B.c.c. and h.c.p. metals have strengths which fall rapidly with increasing temperature below about 0.1 T_M because the flow strength is controlled by the lattice resistance to dislocation glide. Thus $(-\partial\sigma_y/\partial T)$ is large and ϕ is as high as 6.0. Between about 0.1 T_M and 0.2 T_M the thermal softening decreases in magnitude, and from 0.2 to 0.4 T_M, (depending on the strain rate) there is a plateau in which $\phi \sim$ 0.5 to 1.0 (Fig. 10). F.c.c. metals do not show the large values of ϕ at low temperatures. The value of ϕ is easily seen on ordinary deformation maps with axes of σ_s/μ and T/T_M: it is directly related to the slope of the strain-rate contours, shown in Fig. 10.

The work-hardening exponent m falls with increasing temperature. Its value at 300 K is listed in Table 2. Data for pure aluminium, given in the Appendix, suggest an exponential decrease, whereas that for titanium seems to be linear.

The thermal conductivity also decreases with increasing temperature, but, below about 20 K (where m tends to a constant value), K K increases rapidly (by a factor of nearly 100) for pure f.c.c. metals, before dropping towards zero close to 0 K.

Figure 9 shows that this simple approach can be used to predict the approximate position of the adiabatic shear field, including the jump in critical strain-rate (with increasing temperature) when modulus-controlled thermal softening becomes effective. A prediction of the critical strain at 300 K is also possible, using eqns. (16) or (17).

5. FURTHER APPLICATIONS

Adiabatic shear fields have been calculated for mild steel, Ti-6 % Al-4 % V, pure aluminium and commercially pure aluminium (Al 1100); shown in figures 11 to 14. Figure 11 clearly shows the effect of strain-rate on the critical strain. At temperatures above 0.1 T_M, ε_c increases rapidly as the strain-rate drops because of heat losses, but far from the adiabatic limit ε_c increases with increasing strain-rate because the term $\sigma_y \phi$ in eqn. (17) is weakly, but definitely, strain-rate-dependent. The drop in ε_c below 0.1 T_M is due to the drop in C_p with decreasing temperature. The titanium alloy shows the weak strain-rate-dependence (Fig. 12) but the heat loss effect is too small to be seen on the map because the thermal conductivity is very low for this material.

Pure aluminium shows no instability below 0.06 T_M because its thermal conductivity is so high (Fig. 13). Instability does not occur above about 0.12 T_M because the homogeneous heating becomes too great: even at 0.1 T_M the smallest value for ε_c is 200 %.

Figure 14 demonstrates the difference that small alloying additions can make to a metal's thermomechanical properties. Critical strains are still high ($\varepsilon_c \approx 350$ %) but there is no low temperature cut-off due to K and and no high temperature cut-off because m is significantly lower.

6. CONCLUSIONS

The values of critical strain and strain-rate obtained from the theory by the numerical method make it possible to draw four principle conclusions.

1. The thermal diffusion distance (R) is much smaller than the specimen size and is probably related to the microstructure and slip band spacing.

2. Even for pure f.c.c. metals, where the flow stress is not highly strain-rate sensitive, there is a significant effect of strain-rate on the critical strain (ε_c) even in the fully adiabatic condition.

3. The homogeneous heating can easily be large enough to put the material into the power-law creep regime before there is any strain localisation.

4. The thermal softening due solely to the effect of temperature on the shear modulus gives an upper bound to the minimum strain-rate for adiabatic shear. This effect is characteristic of the base metal of any alloy and can not easily be altered.

It must be appreciated that the theory given here contains many approximations and that very little data are available to set the essential constants (like R). But despite these reservations, the method gives a useful way of describing the onset of adiabatic shear and the strain necessary to achieve it. The main qualitative differences between materials are nicely displayed, in a readily accessible way. And as better data become available, the method can be refined and improved.

ACKNOWLEDGEMENTS

We gratefully acknowledge the financial support of the U.S. Army, European Research Office in London.

REFERENCES

American Institute of Physics Handbook (1972), Table 4g-9. McGraw Hill.

Argon, A.S. (1973) in: "The Homogeneity of Plastic Deformation", A.S.M., Metals Park, Ohio, p.161.

Bai, Y. (1981) Albuquerque Conference on High Strain-Rates, to be published.

Backman, M.E. and Finnegan, S.A. (1973) "Metallurgical Effects at High Strain-Rates", Eds. Rohde et al., Plenum, N.Y., p.531.

Backofen, W.A. (1964) in: "Fracture in Engineering Materials", A.S.M., Metals Park, Ohio, p.107.

Baron, H.G. (1956) J. Iron and Steel Inst. 182, 354.

Carslow, H.S. and Jaeger, J.C. (1959) "Conduction of Heat in Solids", Clarendon Press, Oxford.

Considère, M. (1885) Annls. Ponts Chauss 9, 574.

Culver, R.S. (1973) "Metallurgical Effects at High Strain-Rates", Eds. Rohde et al., Plenum, p.519.

Doner, M. and Conrad, H. (1973) Met. Trans. 4, 2809.

Estrin, Y. and Kubin, L.P. (1980) Scripta Met. 14, 1359.

Frost, H.J. and Ashby, M.F. (1982) "Deformation Mechanism Maps", Pergamon Press.

Geiger, G.H. and Poirier, D.R. (1973) Transport Processes in Metallurgy, Addison Wesley, Ch. 7, p.207 et seq.

Garde, A.M., Aigeltinger, E., Woodruff, B.N. and Reed-Hill, R.E. (1975) Met. Trans. 6A, 1183.

Harding, J. (1975) Archiwum Mechaniki Stosowanej 27 (5-6) Warszawa.

Kocks, U.F., Argon, A.S. and Ashby, M.F. (1975) "Thermodynamics and Kinetics of Slip", Prog. Mat. Sci. 19, p.73 et seq.

Kumar, A., Hauser, F.E. and Dorn, J.E. (1968) Acta Met. 16, 1189.

Kumar, A. and Kumble, R.G. (1969) J. Appl. Phys. 40, 3475.

Sargent, P.M. and Ashby, M.F. (1982) Scripta Met. 16 (1982) 1415.

Staker, M.R. (1981) Acta Met. 29, 683.

Tanaka, K., Ogawa, K. and Nojima, T. (1978) IUTAM Symposium on High Strain-Rate Deformation of Metals, Eds. Kawata, K. and Shiori, J., Springer-Verlag, New York. ISBN 0-387-09208-0.

Timothy, S.P. (1982) Personal Communication.

Winter, R.E. (1975) Phil. Mag. 31 (4), p.765.

Woodward, R.L. (1978) Int. J. Mech. Sci. 20, 599.

Wulf, G.L. (1979) Int. J. Mech. Sci. 21, p.713.

Zener, C. and Hollomon, J.H. (1944) J. Appl. Phys. 15, 22.

APPENDIX 1: EVALUATION OF THE ADIABATIC SHEAR CONDITIONS

(a) Numerical Method

When maps are computed numerically, some of the approximations made in the text are unnecessary. Let the yield strength of the material depend on strain, strain-rate and temperature as:

$$\sigma_y\ (\varepsilon,\ \dot{\varepsilon},\ T) = A'\ \mu\ \left(\frac{\varepsilon}{\varepsilon_o}\right)^m \left\{1 + \frac{kT}{\Delta F}\ \ell n\ \left(\frac{\dot{\varepsilon}}{\dot{\varepsilon}_o}\right)\right\} \qquad \text{(A1)}$$

in which the dimensionless quantity A' is given by:

$$A' = \frac{\hat{\tau}_o}{\mu} \qquad \begin{matrix} \text{at} & \varepsilon = \varepsilon_o \\ \text{and} & T = 0\ K \end{matrix} \qquad \text{(A2)}$$

This is simply a combination of eqns. (15) and (29). The equation allows all three partial derivatives that appear in eqn. (9) to be evaluated. Then the two conditions for adiabatic shear can be calculated more precisely, using data given here and in Sargent and Ashby (1982) and Frost and Ashby (1982).

Deformation is modelled at a chosen, constant, strain-rate ($\dot{\varepsilon}$), so that eqn. (10) is valid, starting with the metal at the temperature of the sink (T_s) at a strain of 0.01 %. The strain is increased in steps of 0.01 % and after each increment the flow stress, temperature, thermal softening rate and strain hardening rate are calculated as

differentials of eqn. (A1) and are used in the next increment calculation. At each step the instability criterion:

$$\frac{\partial \sigma_y}{\partial \varepsilon} \leq \frac{\partial \sigma_y}{\partial T} \frac{dT}{d\varepsilon} \tag{A3}$$

is tested and if it is satisfied the critical strain is recorded. If, at any stage, the temperature rises above 0.3 T_M, or if the strain gets ridiculously large (> 10), the calculation is terminated.

In order to determine the effect of heat loss, the temperature increment dT is calculated from:

$$dT = \frac{\sigma_y}{C_p} d\varepsilon - \frac{(T - T_s)}{\tau \dot{\varepsilon}} d\varepsilon \tag{A4}$$

instead of just

$$dT = \frac{\sigma_y}{C_p} d\varepsilon \tag{A5}$$

This illustrates an interesting point, non-adiabatic conditions can actually make instability *more* likely by removing heat and so preventing the temperature from rising into the creep field.

This numerical method gives the instability strain for a given strain-rate and starting temperature. The results depend strongly on the length R. We have selected a value which correctly gives the onset of instability at room temperature and at a known strain-rate, taken from the experiments of Winter (1975), Timothy (1982) and Wulf (1979). The value R = 250 μm gives good agreement for titanium.

For zirconium, aluminium, mild steel and the titanium and zirconium alloys, the same value of R was used (250 μm) as for titanium. Thermal conductivities were found from The AIP Handbook (1972) and, where possible, the variation of the strain hardening index m was taken into account: for titanium m drops linearly with temperature (Harding, 1975) and for aluminium it drops exponentially (Trozera et al., 1957). The data are summarised in Table 3.

TABLE 3: Data for Figs. 6, 7, 11, 12, 13 and 14

Material	m	A	ΔF	ε_o
α-Ti	<0.111 >0.03	1.8×10^{-2}	0.114 μb^3	0.1
α-Zr	0.16	5.6×10^{-3}	0.25 μb^3	0.1
Mild Steel	0.03	8×10^{-3}	0.5 μb^3	1.0
Ti-6 % Al-4 % V	0.114	1.8×10^{-2}	0.5 μb^3	0.01
Aluminium	<0.67 >0.32	3.3×10^{-3}	0.27 μb^3	1.0
Al 1100	0.244	7.9×10^{-3}	0.54 μb^3	1.0

(b) Approximate Method of Equation (34)

Titanium shows adiabatic shear at room temperature for strain-rates, $\dot{\varepsilon}_A^o$, above 10^2 s^{-1} (Timothy, 1982 Winter, 1975 Wulf, 1979). The work-hardening exponents m and m_o are taken from Harding (1975). A linear relationship $m = 0.111 - (8.625 \times 10^{-5})\ T\ K^{-1}$ was fitted

to data for a commercially pure Ti (roughly approximating to ASTM Grade 3 to Grade 4) tested at a strain-rate of 44 s^{-1} between 77 ^{o}K and 660 ^{o}K. Thermal conductivity values were obtained using data points at 4.2 K (K = 5.8 W m^{-1} K^{-1}), 80 K (K = 33 W m^{-1} K^{-1}) and 273 K (K = 20 W m^{-1} K^{-1}) in the AIP handbook. The quantity $(-\partial\sigma/\partial T)$ was taken from Tanaka (1978) and at 664 K this appears to go to zero, thus implying that the predicted limiting strain-rate for adiabatic shear band instability ($\dot{\varepsilon}_A$) would go to infinity. However, ϕ cannot be less than $\left|-\frac{T_M}{\mu_o}\frac{\partial\mu}{\partial T}\right|$, which for α-Ti is 1.2 (Sargent and Ashby, 1982), so $(-\partial\sigma_y/\partial T)$ just drops to 0.08 MPa K^{-1} and $\dot{\varepsilon}_A$ increases to a maximum of 635 s^{-1} (= $10^{2\cdot8}$ s^{-1}) at 665 K. At such a high homologous temperature, *strain-rate stabilisation* will be important and $\dot{\varepsilon}_A$ may well be higher.

APPENDIX 2: EXPERIMENTAL OBSERVATIONS OF ADIABATIC SHEAR IN TITANIUM

There are a number of grades of "commercial" purity titanium, containing, typically, 0.07 wt % N, 0.4 wt % O, 0.1 wt % C and 0.3 wt % Fe. The tensile yield strength depends on the quantity of interstitial, N, O and C and can vary from 250 to 700 MN/m^2. Adiabatic shear has been clearly identified in three studies. The data are summarised in Table 4.

TABLE 4: Adiabatic Shear in CP Titanium

Material	Test Temp (K)	Strain Rate Range (s^{-1})	Ref.
IMI 125	300	$3 \times 10^3 \rightarrow 3 \times 10^4$	Wulf (1979)
IMI 130	300	$\approx 5 \times 10^3$	Timothy (1982)
Low Purity Titanium (probably AMS 4901 Grade 4)	300	$\approx 5 \times 10^4$	Winter (1975)

Wulf (1979), using a modified Hopkinson bar, applied strain-rates in the range $3 \times 10^3/s$ to $3 \times 10^4/s$. He observed Newtonian viscous behaviour above $5 \times 10^3/s$, suggesting drag-controlled plasticity. His data give a drag coefficient $C \approx 1.0 \times 10^7\ s^{-1}$, varying a little with orientation of the sample with respect to the textured sheet from which it was cut. Wulf's micrographs show bands of intensely localised shear.

Timothy (1982) examined the microstructure beneath the indent left by the impact of a high-velocity steel sphere. Etching showed bands of intense shear at room temperature. The strain-rate in such an experiment is less well-defined than that in the Hopkinson bar

experiments but approximate rates can be inferred from the indent dimension and the projectile velocity. In the case of Timothy's experiments, it lies within a factor of 2 of 5×10^3 s^{-1}.

Winter (1975) also indented a commercial-purity titanium, and, like Timothy, found bands of intense localised shear beneath the indenter at high impact velocities. The strain-rates in this case are within a factor of 5 of 5×10^4 s^{-1}.

Woodward (1978), studying the penetration of metal targets by projectiles, also observed signs of adiabatic shear in IMI 125. It is not possible to obtain a strain-rate from his data.

TABLE 2: ROOM TEMPERATURE DATA FOR METALS AND ALLOYS

	T_M (K)	C_p (J m^{-1} K^{-1})	m	σ_y (MN m^{-2})	$\phi = -\frac{T_M}{\sigma_y}\left(\frac{d\sigma_y}{dT}\right)$	ε_c (t)	$\dot{\varepsilon}_A$ (s^{-1}) (u)
Copper	1356 (j)	3.46×10^6 (j)	0.5 (m, f)	55 (d)	3.4 (d)	12.6	4.5×10^4
α-Brass (70/30)	1188 (j)	3.22×10^6 (j)	0.3 (j, m, s)	193 (j)	0.6 (j)	9.9	1.2×10^4
Titanium	1934 (j)	2.36×10^6 (b)	0.17 (e, g, k)	400 (g)	4.1 6.9 (e), 6.0 (g)	(0.3 to 0.5), 0.32	100
Ti-6 % Al-4 % V	1811 (h)	2.59×10^6 (a)	0.08 (e), 0.12 (l, h)	892 (h,l)	2.52 (e)	0.17, 0.25	20
Aluminium	933 (j)	2.44×10^6 (b)	0.325 (m, c)	17 (c)	2.4 (c)	18.1	5.6×10^2
6061-T6 (p)	855 (j)	2.6×10^6 (j)	0.075 (e)	253 (j)	1.68 (e)	0.39	7.4×10^2
Iron	1810 (j)	3.49×10^6 (j)	0.021 (e)	64 (j)	1.9 (e)	1.08	7.5×10^2
4340 (q)	1790 (j)	3.8×10^6 (a)	0.04 to 0.09 (i, r)	905-1380 (i,j,r)	1.4 to 6.8 (e, n, i, r)	0.04-0.32	1.3×10^2

Notes for Table

(a) Smithells, C.J. (1967) Metals Reference Book, 4th Edition.
(b) American Institute of Physics Handbook, Tables 4g-8, 4e-1, 4g-9.
(c) Trozera, T.A., Sherby, O.D., Dorn, J.E., Trans. ASM 49 (1957) 173.
(d) Carreker, R.P., Jnr., Hibberd, W.R., Jnr., Acta Met. 1 (1953) 656-663.
(e) Culver, R.S. in Metallurgical Effects at High Strain Rates, Plenum, N.Y. (1963) 519-530, Eds. Rohde, R.W. et al.
(f) Grewe, H.G., Kappler, E., Phys. Stat. Sol. 6 (1964) 339.
(g) Harding, J., Archiwum Mechaniki Stosowanej 27, 715-735, Warszawa (1975).
(h) Aerospace Structural Metals Handbook, Syracuse University Press (1967), Ed. Sessler, J.G. and Weiss, V. Figures 3111 and 3112.
(i) Staker, M.R., Acta Met. 29 (1981) 683-689.
(j) Metals Handbook, Eighth Edition, ASM.
(k) Measured at a strain (ε_o) of 0.1.
(l) Measured at a strain (ε_o) of 0.01.
(m) These strain-hardening exponents are calculated from published stress/strain curves.
(n) Data for 93 °C, not room temperature.
(o) Data for En 8 Steel (0.42 % C, 0.6 % Mn) which is assumed to be close to that for 4340 steel, see note (q).
(p) 6061 is 1 % Mg, 0.6 % Si, 0.25 % Cu, 0.25 % Cr, balance Al. T6 is the peak-aged condition.
(q) 4340 is 0.38-0.43 % C, 0.6-0.8 % Mn, 0.04 % P, 0.04 % S, 0.2-0.35 % Si, 1.65-2 % Ni, 0.7-0.9 % Cr, 0.2-0.3 % Mo, balance Fe.
(r) This range of values is for 4340 tempered at different temperatures.
(s) Estimate, similar to that for 60/40 brass.

(t) $\varepsilon_c = \frac{m\, C_p\, T_M}{\phi\, \sigma_y}$ (u) $\dot{\varepsilon}_A = \varepsilon_c/\tau$ where $\tau = \frac{C_p\, R^2}{2\alpha K}$ and we take $\alpha = 1$ and $R = 250\ \mu m$.

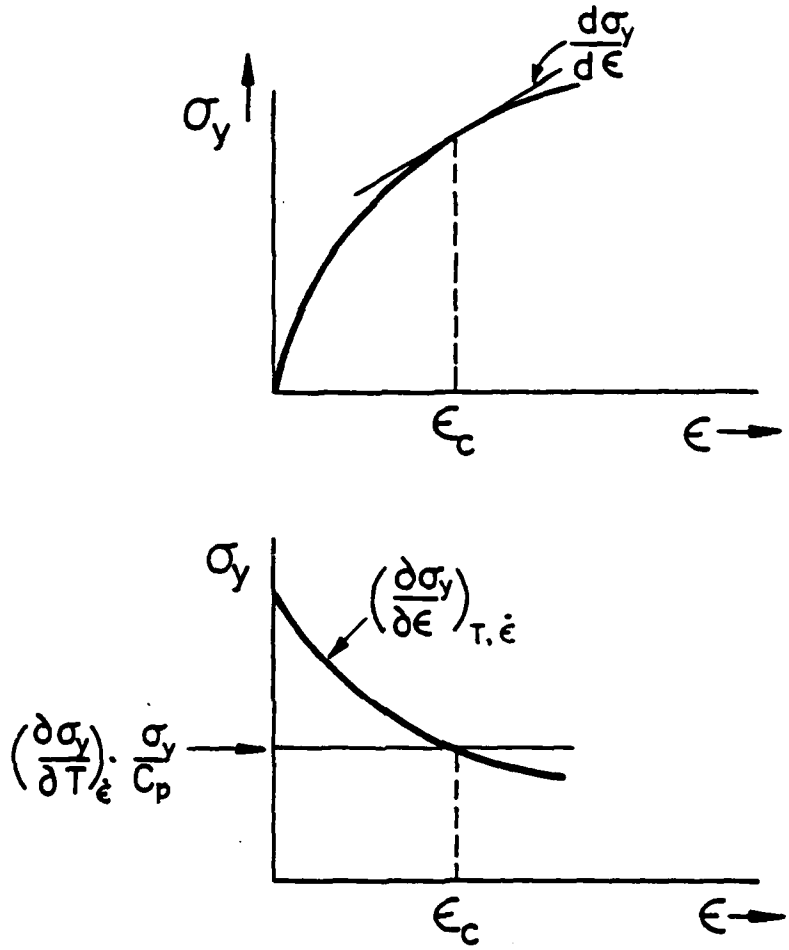

Figure 1: As the material is strained the strain-hardening rate decreases but the rate of thermal-softening remains constant. At ϵ_c deformation becomes unstable and Adiabatic Shear occurs.

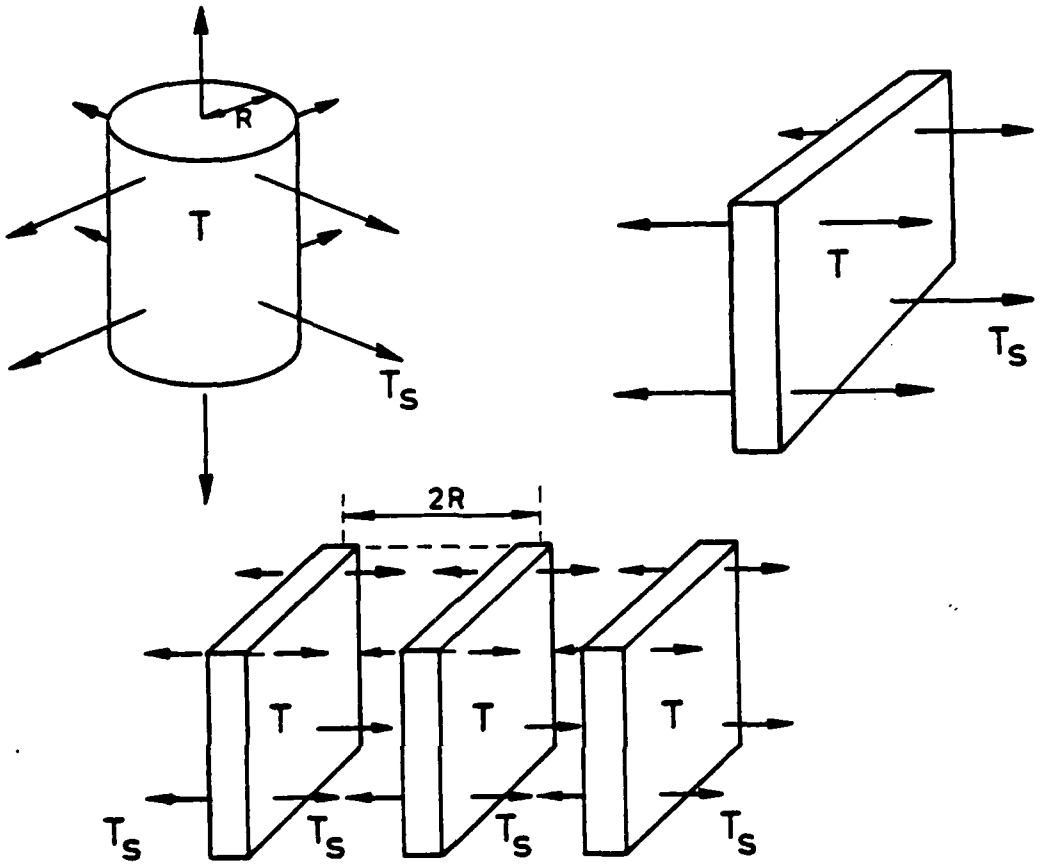

Figure 2: Heat loss from (a) a cylindrical specimen to the environment; (b) from one shear band and (c) from many shear bands, into the bulk of the specimen.

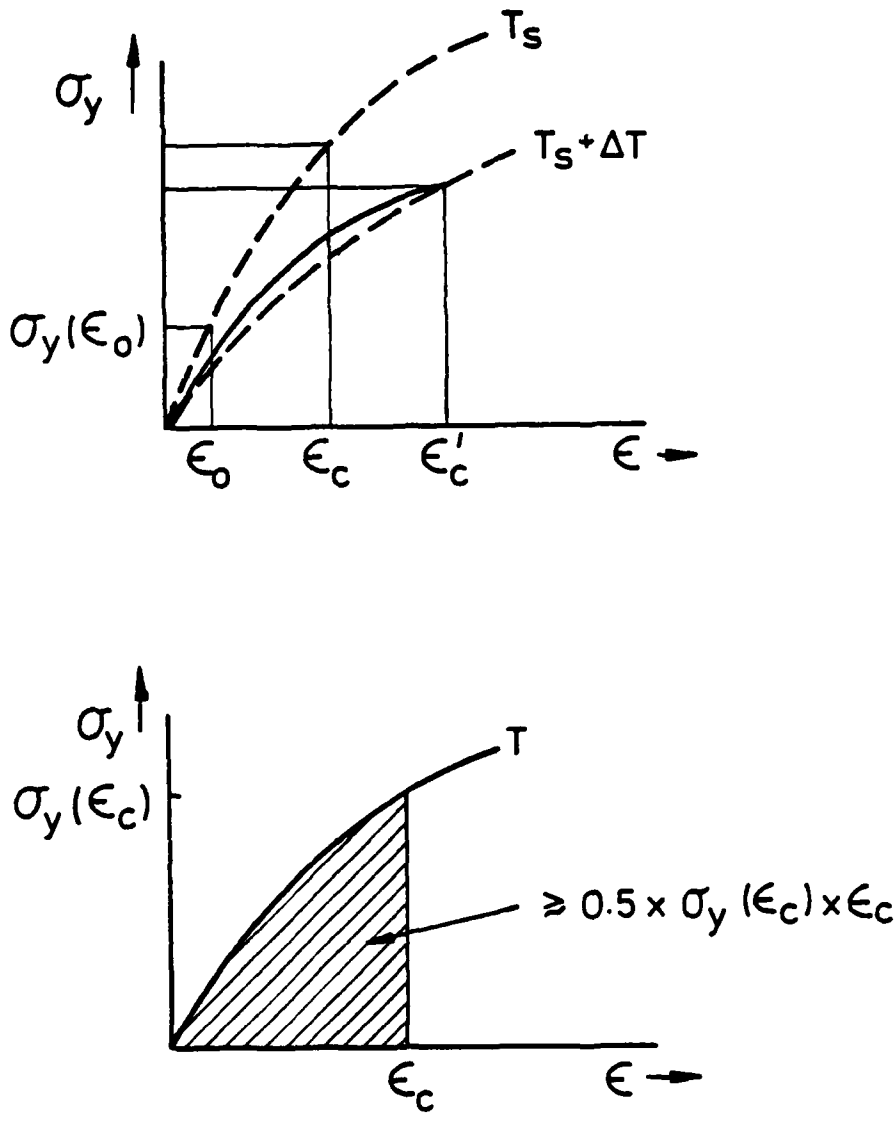

Figure 3: The material heats up homogeneously during straining and softens. As a consequence (if ΔT is significant) the material is stabilised with respect to shear instability and the critical strain increases from ϵ_c to ϵ_c'. The yield stress here is defined as the flow stress at a strain of ϵ_o (see Table 2).

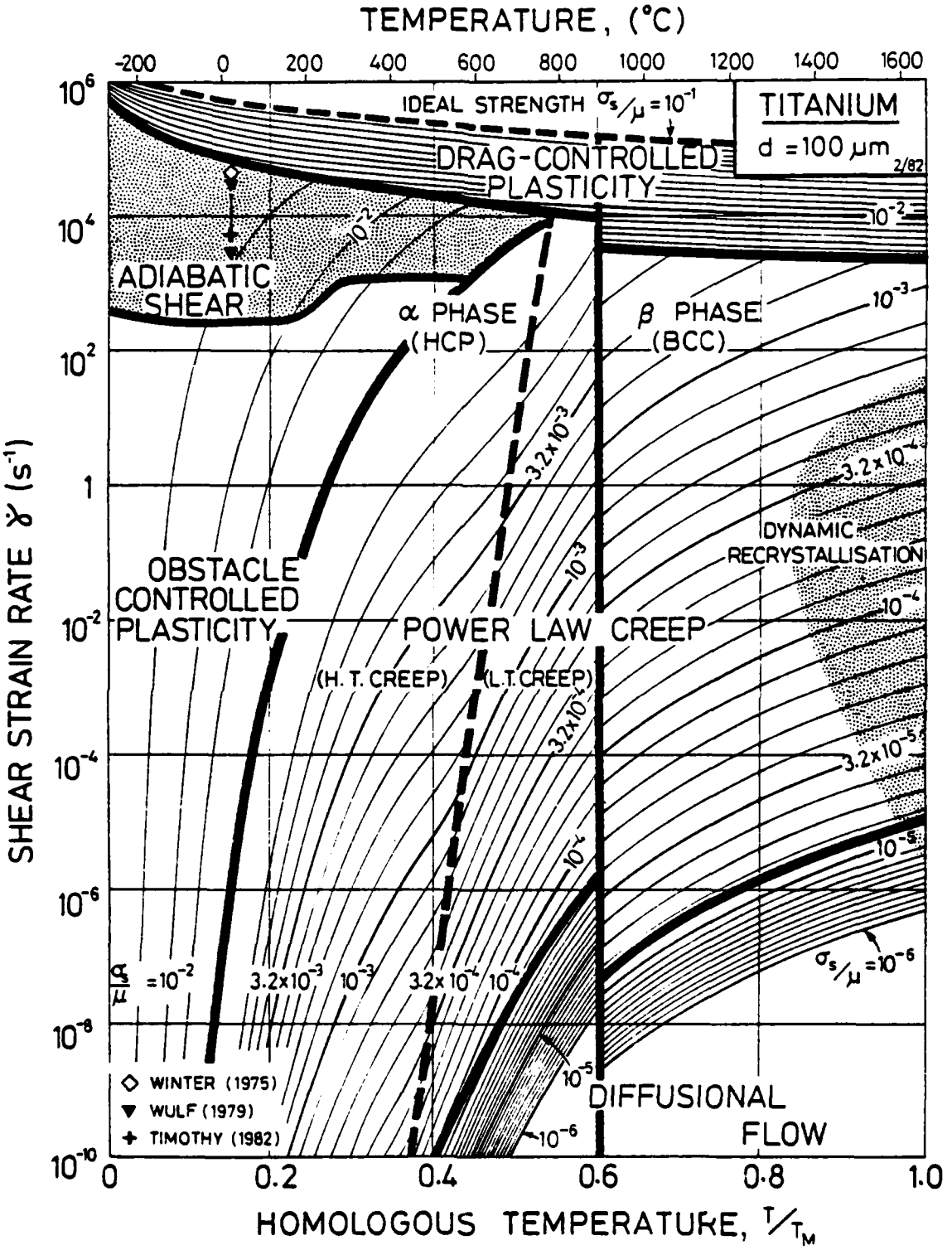

Figure 4: Strain rate/homologous temperature deformation map for titanium. The adiabatic shear field position by the numerical method (see Fig. 6).

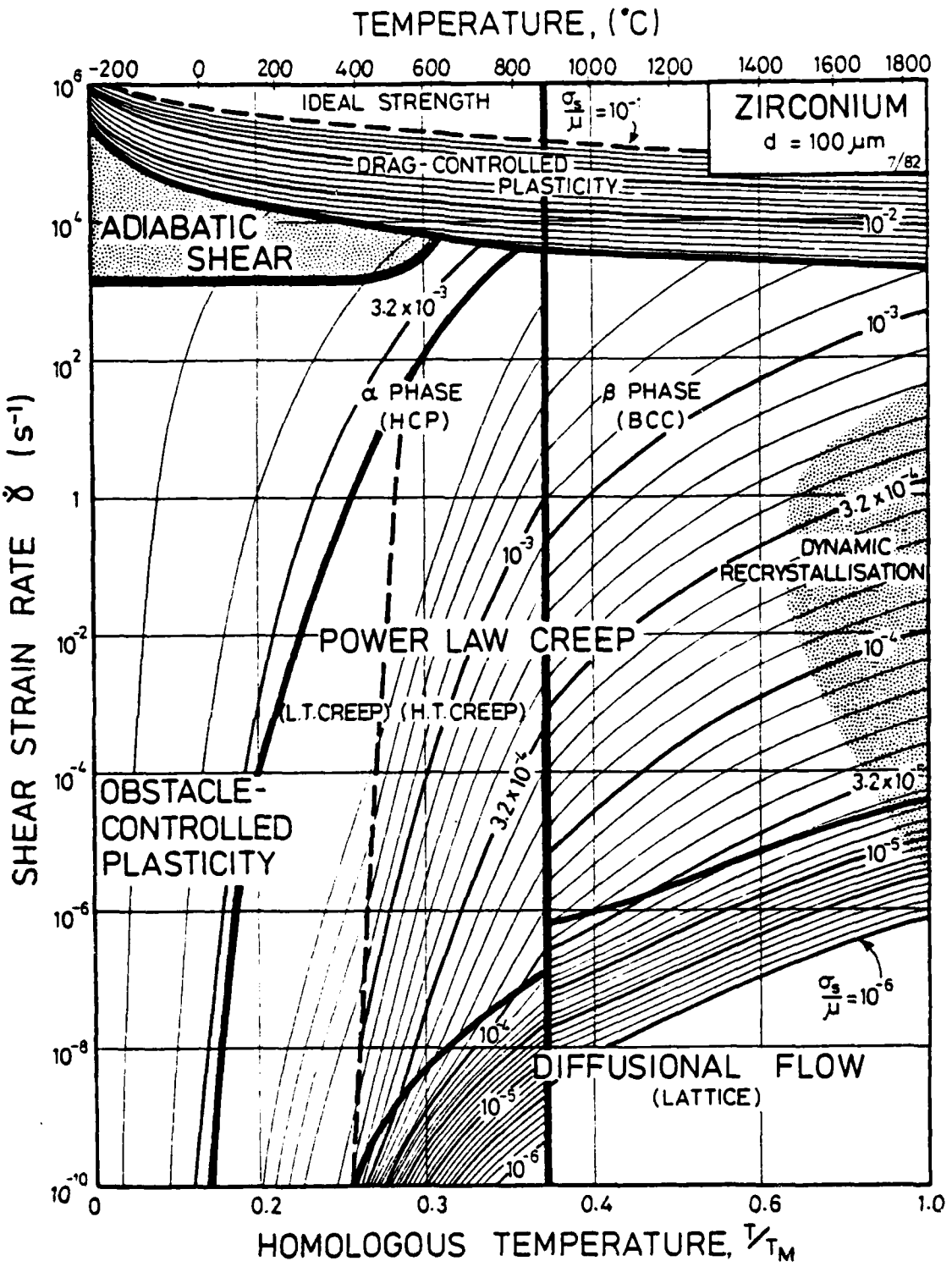

Figure 5: Strain rate/homologous temperature deformation map for zirconium. The adiabatic shear field position is determined by the numerical method (Fig. 7).

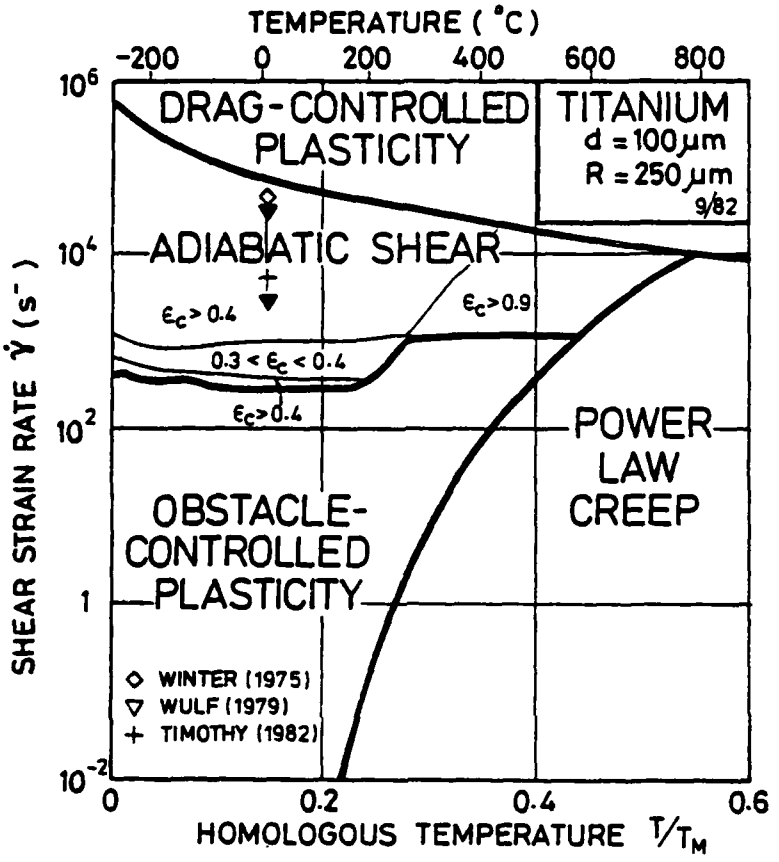

Figure 6: Adiabatic shear field on a partial α-titanium deformation map showing critical strain contours determined by the numerical method.

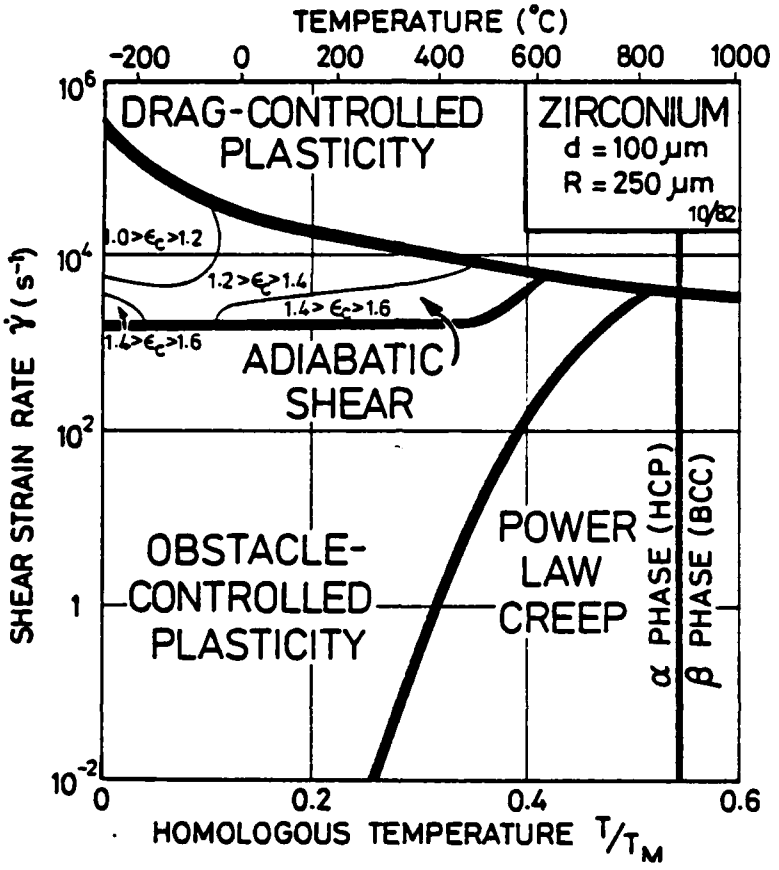

Figure 7: Adiabatic shear field on a partial α-zirconium deformation map showing critical strain contours determined by the numerical method.

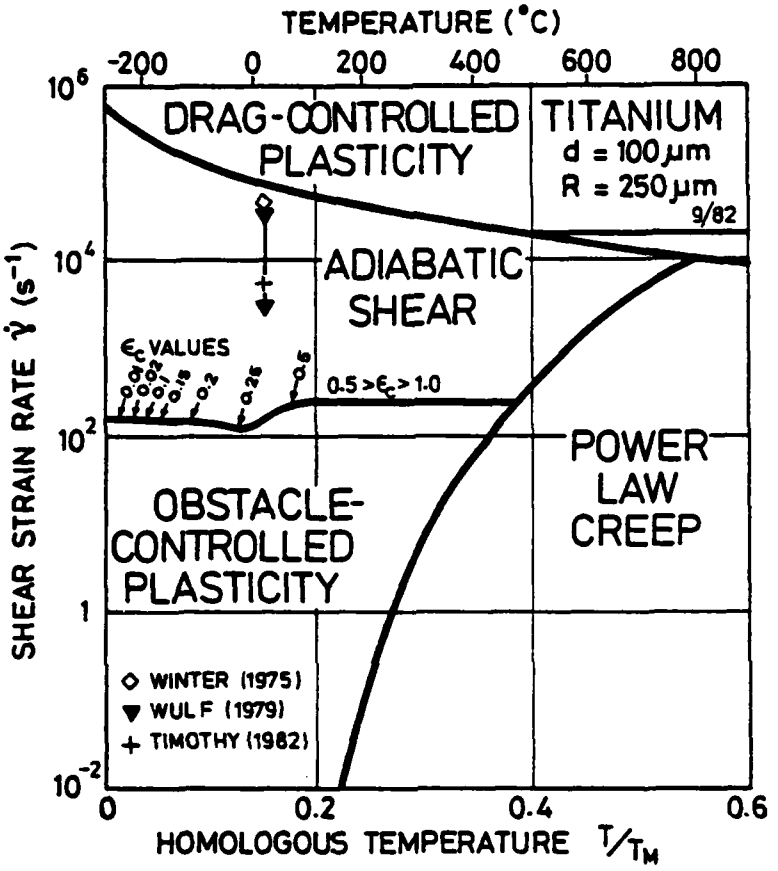

Figure 8: Adiabatic shear field on a partial α-titanium deformation map with the minimum strain rate calculated using $\dot{\epsilon} = \epsilon_c/\tau$ (see text).

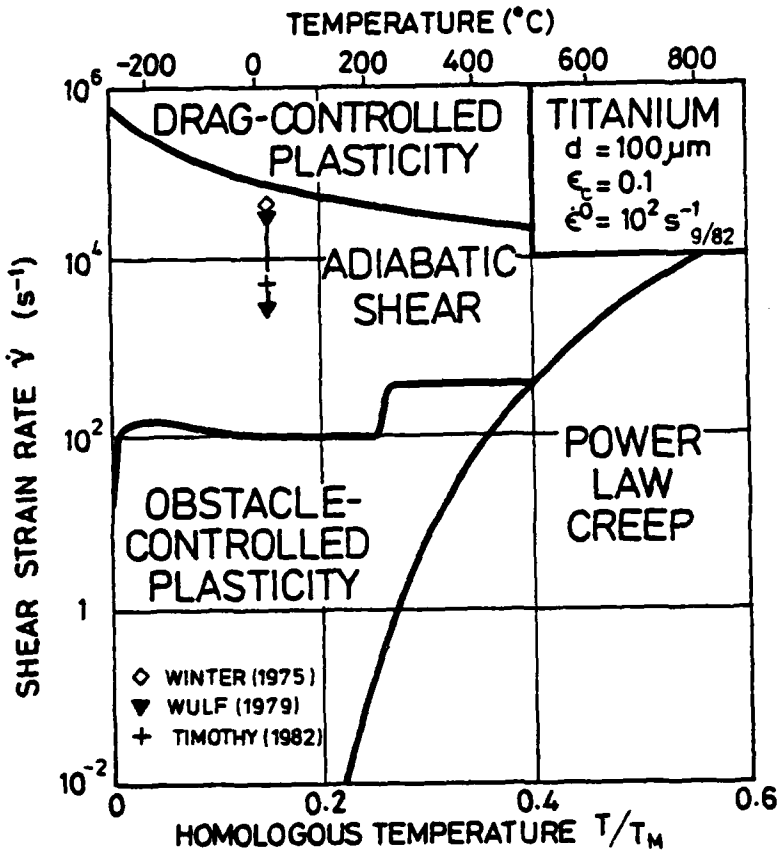

Figure 9: Adiabatic shear field on a partial α-titanium deformation map with the minimum strain rate calculated using eqn. (34).

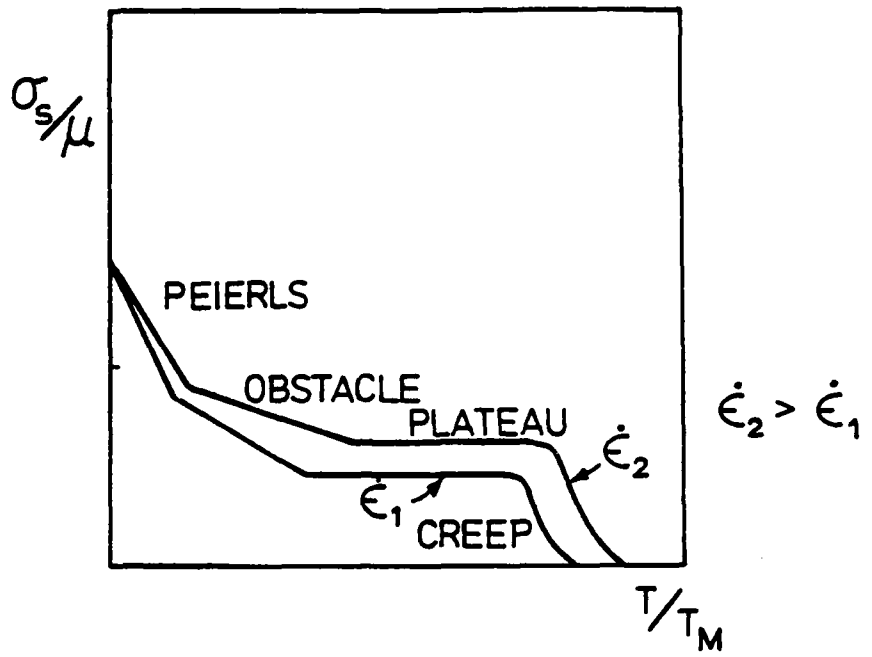

Figure 10: A diagram of part of a typical normalised stress/ homologous temperature deformation map showing a plateau where the strength scales as the modulus because the deformation is transitional between the glide and the glide + climb (creep) mechanisms.

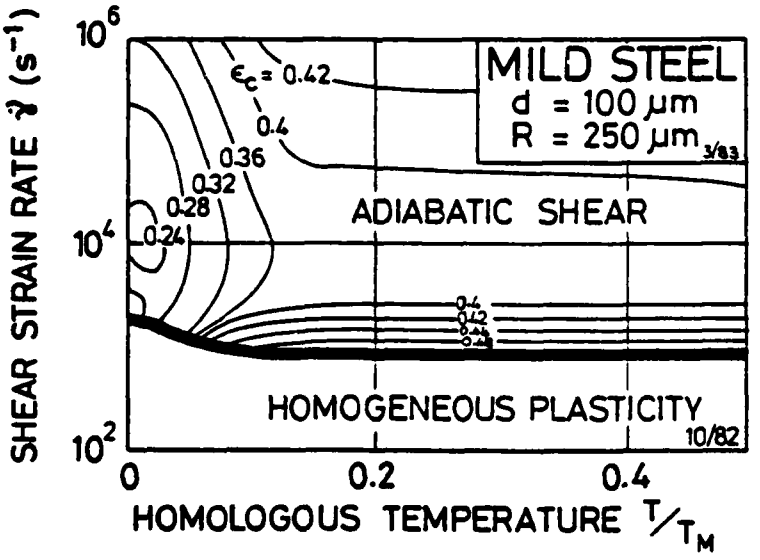

Figure 11: Adiabatic shear field on a partial mild steel deformation map showing critical strain contours determined by the numerical method.

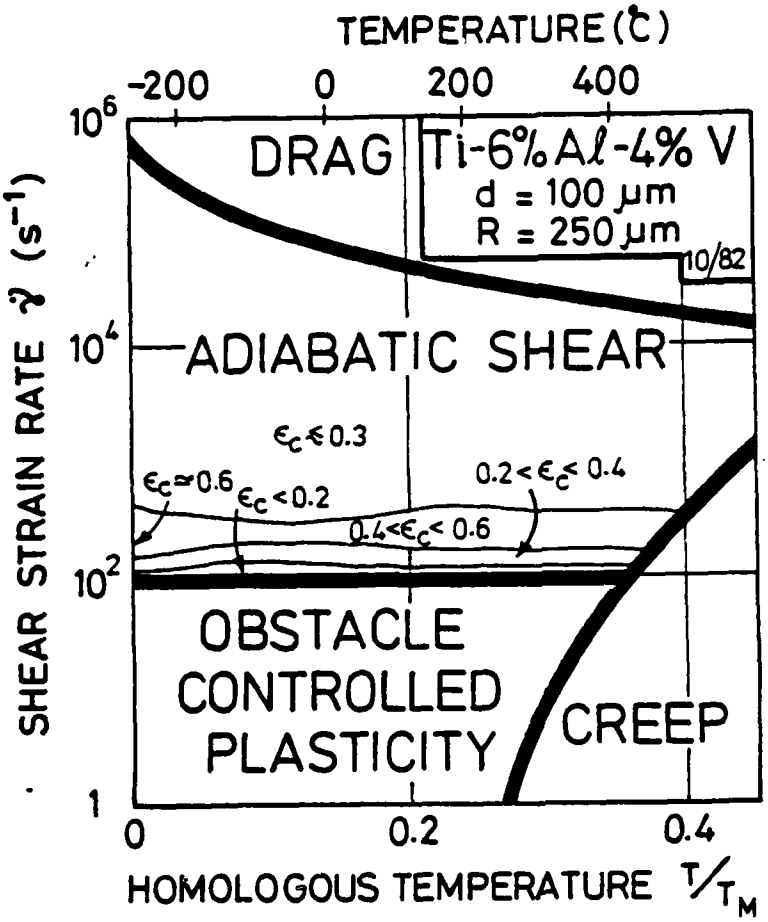

Figure 12: Adiabatic shear field on a partial Ti-6 % Al-4 % V deformation map showing critical strain contours determined by the numerical method.

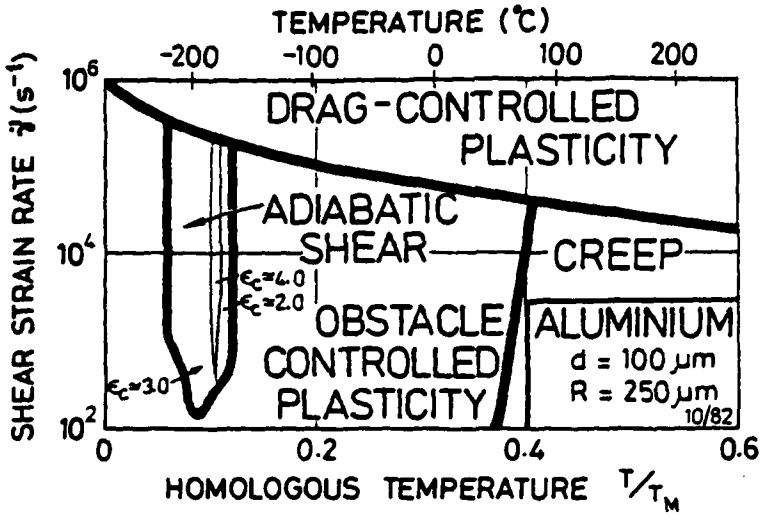

Figure 13: Adiabatic shear field on a partial aluminium deformation map showing critical strain contours determined by the numerical method.

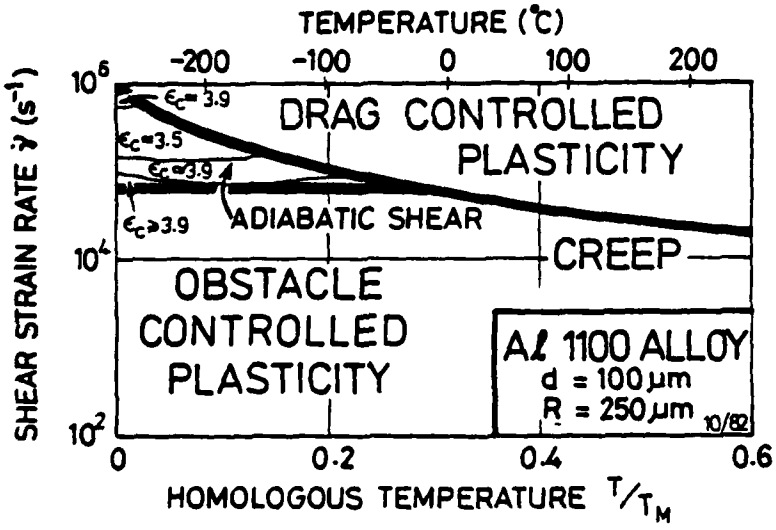

Figure 14: Adiabatic shear field on a partial aluminium alloy (Al 1100) deformation map showing critical strain contours determined by the numerical method.

END

FILMED

6-83

DTIC